PROCEEDINGS A

rspa.royalsocietypublishing.org

Research

Article submitted to journal

Subject Areas:

xxxxx, xxxxx, xxxx

Keywords:

xxxx, xxxx, xxxx

Author for correspondence:

Ory Schnitzer

e-mail: o.schnitzer@imperial.ac.uk

Slender-body theory for plasmonic resonance

Matias Ruiz[1] and Ory Schnitzer[1]

[1]Department of Mathematics, Imperial College London, London SW7 2AZ, UK

We develop a slender-body theory for plasmonic resonance of slender metallic nanoparticles, focusing on a general class of axisymmetric geometries with locally paraboloidal tips. We adopt a modal approach where first one solves the plasmonic eigenvalue problem, a geometric spectral problem which governs the surface-plasmon modes of the particle; then, the latter modes are used, in conjunction with spectral-decomposition, to analyse localized-surface-plasmon resonance in the quasi-static limit. We show that the permittivity eigenvalues of the axisymmetric modes are strongly singular in the slenderness parameter, implying widely tunable, high-quality-factor, resonances in the near-infrared regime. For that family of modes, we use matched asymptotics to derive an effective eigenvalue problem, a singular-nonlocal Sturm–Liouville problem, where the lumped one-dimensional eigenfunctions represent axial voltage profiles (or charge line densities). We solve the effective eigenvalue problem in closed form for a prolate spheroid and numerically, by expanding the eigenfunctions in Legendre polynomials, for arbitrarily shaped particles. We apply the theory to plane-wave illumination in order to elucidate the excitation of multiple resonances in the case of non-spheroidal particles.

1. Introduction

Metallic nanoparticles exhibit extraordinary optical properties when illuminated by light in the visible regime [1]. Specifically, when the incident radiation resonantly excites localized-surface plasmons, namely, collective oscillations of electron-surface charge and electric field, absorption, scattering and the magnitude of the electric near-field are enhanced. This phenomenon, known as localized-surface-plasmon resonance, holds promise for a wide range of applications including bio-sensing, targeted heating, nonlinear optics, metamaterials and microfluidics.

THE ROYAL SOCIETY PUBLISHING

Extreme nanometallic geometries are commonly used in plasmonic applications in order to tune resonance frequencies and generate giant field enhancements [2]. Accordingly, in recent years the plasmonic properties of such structures have been extensively investigated. A range of analytical methods, including separation of variables, transformation optics, matched asymptotic expansions and layer-potential techniques, have been used to study idealised singular geometries, involving sharp edges and touching particles [3–8], as well as nearly singular, or multiple-scale, geometries, with a particular emphasis on nearly touching particles and particles in close proximity to a substrate [9–19].

Our interest here is in another important family of multiple-scale geometries: slender particles in three dimensions. Owing to their unique optical properties, slender metallic nanoparticles have been widely employed as plasmonic rulers [20], orientation sensors [21], nano-antennas [22], bio-sensors [23, 24] and nanoscale heating devices [25]. The use of high-aspect-ratio particles in nanoplasmonics is primarily based on the excitation of low-order *longitudinal* modes; the latter are characterized by long wavelengths (roughly proportional to aspect ratio) and surface-charge densities that vary mainly along the long scale of the geometry. Such longitudinal modes efficiently couple to both light and near-field sources, enabling low-frequency (near-infrared), high-quality-factor, optical resonances [26–32].

In comparison to configurations of nearly touching particles, high-aspect-ratio particles have received far less theoretical attention; their optical properties have typically been studied numerically, or based on classical analytical solutions for ellipsoids [33, 34]. The latter solutions are exact in the quasi-static limit but cumbersome and highly specialized; for example, ellipsoids support only a single longitudinal mode that is *dipolar*, i.e., able to efficiently couple with incident light. Accordingly, and following recent singular-perturbation analyses of nearly touching particles [14–17], we propose to *asymptotically* study the plasmonic properties of generically shaped elongated particles in the high-aspect-ratio, or *slender-body*, limit. Our goal is not just to develop a convenient calculation scheme in this limit, but also to gain physical insight into the dependence upon shape and aspect ratio in particular.

To this end, we shall build on *slender-body theory* (SBT), a classical asymptotic methodology developed mainly in the context of Stokes [35–39] and potential [40–43] flows; SBT has had immense impact on multiple scientific and engineering fields including aerodynamics, hydrodynamics, electrostatics and transport phenomena and remains particularly influential in the field of biological microhydrodynamics [44]. SBT is based on the fact that in the slender-body limit the particle geometry degenerates to a zero-thickness curve; the disturbance caused by the particle is accordingly considered to arise from singularities distributed along that curve. The minimal appropriate distribution of singularities, for a given order of approximation, is determined by asymptotically matching the above *outer* limit, valid on the scale of the particle, with an *inner* expansion valid at distances from the centreline scaling with particle thickness [37, 38, 45]. The simplification is that in the inner limit the particle is locally approximated by an infinite cylinder whereas in the outer limit the solution satisfies matching requirements along the particle's centreline.

Our goal is to develop and demonstrate the efficacy of a slender body theory for localized-surface-plasmon resonance. To this end, it will be convenient to adopt a modal approach based on spectral decomposition. In particular, in the quasi-static limit pertinent to subwavelength metallic nanoparticles in the visible range [33, 46], the established modal approach entails solving the so-called *plasmonic eigenvalue problem*, a purely geometric spectral problem governing the permittivity eigenvalues and corresponding eigenfunctions of the particle [34, 47–58]. Once the latter problem is solved, the frequency response of an arbitrary *lossy* metallic nanostructure, for arbitrary external forcing, is explicitly provided in terms of the geometry's eigenvalues and eigenfunctions. At near-resonance frequencies often a single mode dominates the spectral expansion; the modal approach is thus not only efficient but also offers unique insight by providing a clear linkage between physical resonances and mathematical eigenfunctions.

In light of the above, the key step towards developing our SBT for plasmonic resonance will be to asymptotically solve the plasmonic eigenvalue problem, with the slenderness of the shape providing the single small parameter. For the sake of simplicity, we focus here on axisymmetric particles, in which case the longitudinal modes are the lower-order axisymmetric ones. In particular, we consider a general class of axisymmetric geometries for which the thickness profile varies on a single scale (the long scale of the particle) and the tips are locally paraboloidal. Non-axisymmetric modes and geometries with blunt tips are both briefly addressed though their detailed analysis is left for future work, along with other extensions to more general geometries and physical models.

It is useful to mention a distinction commonly made between *local* and *nonlocal* SBT. Local SBT are much simpler but typically provide only a crude approximation, with a relative error scaling inversely with the logarithm of the slenderness parameter. In contrast, nonlocal SBT typically provide an accurate approximation, algebraic in the slenderness parameter; the penalty is that a nonlocal integral operator enters the formulation. In the context of Stokes flows, for example, local and nonlocal SBT physically differ in whether hydrodynamic interactions between different segments of the body are accounted for. As it turns out, the plasmonic eigenvalue problem is nonlocal even at the level of a logarithmic approximation, owing to the appearance of a differential operator relating charge and voltage. In our analysis we aim to derive an algebraically accurate SBT.

The paper is organized as follows. In §2 we formulate the general problem of scattering from a metallic nanoparticle and discuss its spectral solution in terms of the eigen-solutions of the plasmonic eigenvalue problem. In §3 we study the axisymmetric modes in the slender-body limit, arriving at an equivalent one-dimensional eigenvalue problem. In §4 we find closed form solutions to the effective eigenvalue problem in the case of a prolate spheroid and develop a semi-analytical scheme to efficiently compute solutions in the case of an arbitrary smooth body of revolution; the non-axisymmetric modes are briefly discussed in §5. In §6 we use the spectral solution together with the asymptotic eigenvalues and eigenfunctions to study plane-wave illumination for both spheroids and non-spheroids. We conclude in §7 with a discussion of possible applications, generalizations and extensions to our theory.

2. Problem formulation

(a) Quasi-static scattering problem

Consider the scattering problem wherein a metallic nanoparticle surrounded by a homogeneous dielectric medium is subjected to plane-wave illumination and perhaps also a distribution of near-field sources. We assume the quasi-static limit and work at constant angular frequency ω, adopting the usual language of phasors. Thus, the electric potential $\varphi(\mathbf{x})$ satisfies

$$\boldsymbol{\nabla}\cdot(\epsilon\boldsymbol{\nabla}\varphi)=\frac{i}{\epsilon_0\omega}\boldsymbol{\nabla}\cdot\mathbf{J}, \tag{2.1}$$

where the relative permittivity $\epsilon(\mathbf{x};\omega)$ is a piecewise constant function of the position vector $\mathbf{x}$, equal to the complex relative permittivity $\epsilon_c(\omega)$ inside the inclusion and the positive relative permittivity ϵ_b in the background medium; furthermore, ϵ_0 is the vacuum permittivity and $\mathbf{J}(\mathbf{x})$ is the prescribed current-source density, which is assumed to vanish inside the particle. The near-field problem is closed by the far-field condition

$$\varphi\sim-\mathbf{E}_\infty\cdot\mathbf{x}+o(1)\quad\text{as}\quad|\mathbf{x}|\to\infty, \tag{2.2}$$

where $\mathbf{E}_\infty$ is the amplitude of the incident plane wave and we specify the error as $o(1)$ in order to eliminate a physically immaterial additive freedom in the potential.

We note that (2.1) corresponds to the long-wavelength limit of Maxwell's equations, whereas (2.2) arises from matching the scattered field with outward-propagating solutions of Maxwell's equations on the large scale of the wavelength [46].

(b) The plasmonic eigenvalue problem

The plasmonic eigenvalue problem consists of finding those values (eigenvalues) of ϵ_c/ϵ_b for which there exist non-trivial homogeneous solutions to (2.1)–(2.2) with both $\mathbf{J}(\mathbf{x})$ and $\mathbf{E}_\infty$ set to zero. It is well known that the eigenvalues are scale invariant, negative-real and for smooth shapes discretely distributed with an accumulation point at -1. We denote the eigenvalues by $\mathcal{E}^{(n)}$, where the index n counts multiplicities. Without loss of generality, we shall always choose the corresponding eigenfunctions $\varphi^{(n)}(\mathbf{x})$ to be real valued, dimensionless and to attenuate at large distances. We shall also choose the eigenfunctions so as to satisfy the orthogonality relation

$$\int \boldsymbol{\nabla}\varphi^{(n)} \cdot \boldsymbol{\nabla}\varphi^{(m)} dV = 0 \quad \forall n \neq m, \tag{2.3}$$

where the integral is taken over the *interior* volume of the particle. Any two eigenfunctions corresponding to different eigenvalues necessarily satisfy (2.3) [52]; if there are degenerate eigenvalues then the set of eigenfunctions can still be chosen so as to satisfy (2.3).

(c) Modal solution to the scattering problem

We return to the scattering problem formulated in §§2(a), assuming that the plasmonic eigenvalue problem described in §§2(b) has been solved for the prescribed shape of the particle. An explicit modal solution to the scattering problem is then given as [34, 47, 54–56]

$$\varphi(\mathbf{x}) = \varphi^{(i)}(\mathbf{x}) + \sum_{n=0}^{\infty} \frac{\epsilon_c/\epsilon_b - 1}{\epsilon_c/\epsilon_b - \mathcal{E}^{(n)}} \frac{\int \boldsymbol{\nabla}\varphi^{(i)} \cdot \boldsymbol{\nabla}\varphi^{(n)}\, dV}{\int \boldsymbol{\nabla}\varphi^{(n)} \cdot \boldsymbol{\nabla}\varphi^{(n)}\, dV} \varphi^{(n)}(\mathbf{x}), \tag{2.4}$$

where $\varphi^{(i)}(\mathbf{x})$ is the solution to the electric potential in the absence of the particle and the volume integrals are taken over the interior of the particle.

Starting from the modal solution (2.4), many important optical quantities can be calculated, e.g., optical cross sections, field enhancements and the local density of states [34, 55, 59]. Ignoring a possible dependence of the incident potential $\varphi^{(i)}(\mathbf{x})$ upon frequency, both the *overlap* integral in the numerator and the *normalization* integral in the denominator are frequency independent. The frequency response of the nanoparticle thus enters solely through the metal's complex permittivity $\epsilon_c(\omega)$; the latter is available empirically for given metals [60] but for the sake of illustration it is useful to also consider the Drude model

$$\epsilon_c(\omega) = 1 - \frac{\omega_p^2}{\omega^2 + i\gamma\omega}, \tag{2.5}$$

wherein ω_p is the plasma frequency (typically in the ultraviolet range) and γ is a loss parameter. Note that $\mathrm{Re}(\epsilon_c(\omega)) < 0$ for ω below approximately ω_p.

An important feature of the modal solution is that it suggests that the nth mode may become resonantly enhanced for frequencies such that $\epsilon_c(\omega)/\epsilon_b \approx \mathcal{E}^{(n)}$. Since the eigenvalues are real, whereas $\epsilon_c(\omega)$ is complex, such resonant enhancements are always bounded. Intuitively, a weakly damped resonance due to excitation of the nth mode is only possible for sufficiently weak losses such that $\mathrm{Im}(\epsilon_c(\omega)/\epsilon_b)/\mathcal{E}^{(n)} \ll 1$ for $\mathrm{Re}(\epsilon_c(\omega)/\epsilon_b) \approx \mathcal{E}^{(n)}$; note that for negative-large permittivity eigenvalues, corresponding to low frequencies [cf. (2.5)], this condition does not actually demand small $\mathrm{Im}(\epsilon_c(\omega))$. The occurrence of resonances and their sharpness also depend upon the overlap of the excited modes with the incident field and interference effects; the latter are especially important in the dense part of the spectrum ($\mathcal{E}^{(n)} \approx -1$), corresponding to frequencies $\omega \approx \omega_p$.

(d) Axisymmetric particles

We henceforth consider the particle geometry to be a smooth body of revolution of length $2a$. As shown in Fig. 1, we introduce cylindrical coordinates (ar, az, θ) and write the particle's boundary

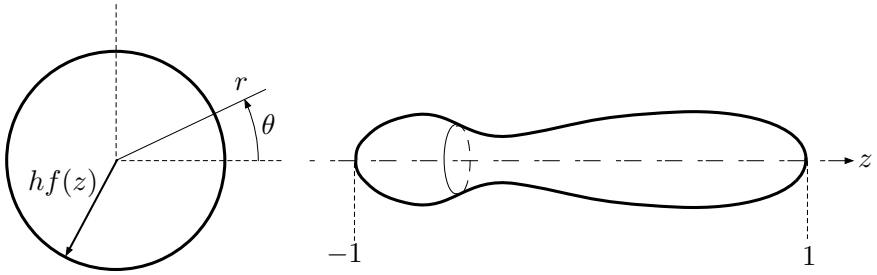

Figure 1. Dimensionless schematic of the axisymmetric particle geometry. Our interest is in slender particles ($h \ll 1$).

as

$$r = hf(z) \quad \text{for} \quad -1 \le z \le 1, \tag{2.6}$$

where h is a dimensionless slenderness parameter and $f(z) > 0$ is a thickness function that is independent of h. We assume that the tips of the particle are locally paraboloidal, so that

$$f(z) \sim \kappa_{\pm}(z \mp 1)^{1/2} \quad \text{as} \quad z \to \pm 1, \tag{2.7}$$

where $\kappa_{\pm}$ are two positive constants.

Consider the plasmonic eigenvalue problem for the above family of geometries. Given the axial symmetry, we write the eigenvalues and eigenpotentials in the form

$$\mathcal{E}^{(n,\pm m)}, \quad \varphi^{(n,\pm m)}(\mathbf{x}) = \psi^{(n,m)}(r,z) \begin{cases} \cos(m\theta) \\ \sin(m\theta) \end{cases}, \tag{2.8}$$

where instead of a single index n we use $(n, \pm m)$, where $m = 0, 1, 2, \ldots$ is the azimuthal number, n now enumerating the modes for fixed m and the sign $\pm$ indicating the $\cos(m\theta)$ and $\sin(m\theta)$ solution, respectively. According to our convention of working with real-valued eigen-potentials, the reduced potentials $\psi^{(n,m)}$ are also real valued. In what follows, when there is no risk of confusion we shall omit the superscript (n, m) and adopt a convention where $\bar{\psi}$ and ψ respectively represent the reduced potential in the interior and exterior of the particle.

We can now formulate a dimensionless eigenvalue problem for fixed m. It follows from (2.1), with $\mathbf{J}$ set to zero, that the reduced potentials $\bar{\psi}$ and ψ satisfy Laplace's equations

$$\frac{\partial^2 \bar{\psi}}{\partial r^2} + \frac{1}{r}\frac{\partial \bar{\psi}}{\partial r} + \frac{\partial^2 \bar{\psi}}{\partial z^2} - \frac{m^2}{r^2}\bar{\psi} = 0, \tag{2.9a}$$

$$\frac{\partial^2 \psi}{\partial r^2} + \frac{1}{r}\frac{\partial \psi}{\partial r} + \frac{\partial^2 \psi}{\partial z^2} - \frac{m^2}{r^2}\psi = 0, \tag{2.9b}$$

respectively in the interior and exterior of the particle; furthermore, at the particle boundary we have continuity

$$\bar{\psi} = \psi \tag{2.10}$$

and displacement continuity

$$\mathcal{E}\left(\frac{\partial \bar{\psi}}{\partial r} - h\frac{df}{dz}\frac{\partial \bar{\psi}}{\partial z}\right) = \frac{\partial \psi}{\partial r} - h\frac{df}{dz}\frac{\partial \psi}{\partial z}, \tag{2.11}$$

where $\mathcal{E}$ is the permittivity eigenvalue. The eigenvalue problem is closed by the attenuation condition

$$\psi \to 0 \quad \text{as} \quad r^2 + z^2 \to \infty, \tag{2.12}$$

which follows from (2.2) with $\mathbf{E}_\infty$ set to zero.

(e) Slender-body limit

Our goal is to study the plasmonic properties of high-aspect-ratio particles for which the slenderness parameter h is small. The first step is to obtain asymptotic solutions to the dimensionless plasmonic eigenvalue problem (2.9)–(2.12) in the limit $h \to 0$. The asymptotic analysis in the axisymmetric case $m = 0$ turns out to be inherently different from that in the non-axisymmetric case $m \neq 0$. We shall therefore consider these two cases separately, focusing on the former, which corresponds to the longitudinal modes discussed in the introduction. The second step is to use the asymptotic eigen-solutions in order to approximate the modal solution (2.4) for small h.

In our analysis of the eigenvalue problem, we will employ the method of matched asymptotic expansions [40, 45], separately analysing an inner region close to the particle's symmetry axis and an outer region that describes the potential on the scale of the particle; we will also need to consider additional asymptotic regions close to the particle tips.

A common feature of slender-body theory is that the asymptotic expansions include logarithms, alongside algebraic powers, of the slenderness parameter h. Unless where explicitly stated otherwise, we adopt the notion of collecting together terms that are only logarithmically separated from each other so as to ensure a relative error that is algebraic in h [38, 40, 61].

3. Axisymmetric modes

(a) Inner limit and singular eigenvalue scaling

Consider first the axisymmetric case $m = 0$. On the cross-section scale, the particle is locally approximated by an infinite circular cylinder. To take advantage of this, we consider the *inner limit*: $h \to 0$ with the inner coordinates

$$\rho = r/h, \quad z \in (-1, 1) \tag{3.1}$$

fixed. Laplace's equation (2.9) accordingly becomes

$$\frac{1}{\rho}\frac{\partial}{\partial \rho}\left(\rho \frac{\partial \bar{\psi}}{\partial \rho}\right) + h^2 \frac{\partial^2 \bar{\psi}}{\partial z^2} = 0 \quad \text{for} \quad \rho < f(z), \tag{3.2a}$$

$$\frac{1}{\rho}\frac{\partial}{\partial \rho}\left(\rho \frac{\partial \psi}{\partial \rho}\right) + h^2 \frac{\partial^2 \psi}{\partial z^2} = 0 \quad \text{for} \quad \rho > f(z). \tag{3.2b}$$

Similarly, (2.10) and (2.11) provide the boundary conditions

$$\bar{\psi} = \psi \quad \text{at} \quad \rho = f(z) \tag{3.3}$$

and

$$\mathcal{E}\left(\frac{\partial \bar{\psi}}{\partial \rho} - h^2 \frac{\partial f}{\partial z}\frac{\partial \bar{\psi}}{\partial z}\right) = \frac{\partial \psi}{\partial \rho} - h^2 \frac{\partial f}{\partial z}\frac{\partial \psi}{\partial z} \quad \text{at} \quad \rho = f(z), \tag{3.4}$$

respectively. There is a slight abuse of notation here as we are now considering ψ and $\bar{\psi}$ as functions of the inner coordinates.

Since ψ and $\bar{\psi}$ are determined only up to a multiplicative constant, we may assume without loss of generality that they are $O(1)$ in the inner region. This, together with the continuity condition (3.3) suggests the expansions

$$\psi(\rho, z; h) \sim \psi_0(\rho, z; h) + \cdots \quad \text{as} \quad h \to 0, \tag{3.5a}$$

$$\bar{\psi}(\rho, z; h) \sim \bar{\psi}_0(\rho, z; h) + h^2 \bar{\psi}_2(\rho, z; h) + \cdots \quad \text{as} \quad h \to 0, \tag{3.5b}$$

where it is to be understood that the h dependence of the functions on the right hand side is at most logarithmic. The need to consider the algebraic correction in (3.5*b*) will soon become apparent.

The eigenvalue $\mathcal{E}$ appearing in (3.4) is a key unknown and its scaling with h is determined as part of the problem. To this end, consider the leading-order balance of (3.2*a*):

$$\frac{1}{\rho}\frac{\partial}{\partial\rho}\left(\rho\frac{\partial\bar{\psi}_0}{\partial\rho}\right)=0. \tag{3.6}$$

Integrating with respect to ρ and requiring $\bar{\psi}_0$ to be bounded shows that the latter function is independent of ρ. We accordingly write

$$\bar{\psi}_0(\rho,z;h)=v(z;h), \tag{3.7}$$

where $v(z;h)$ represents the cross-sectionally uniform voltage along the particle axis. With (3.5) and (3.7), the displacement boundary condition (3.4) implies that the eigenvalue possesses the singular asymptotic expansion

$$\mathcal{E}\sim-\frac{\alpha(h)}{h^2}+\cdots\quad\text{as}\quad h\to0, \tag{3.8}$$

where α is a reduced eigenvalue which depends at most logarithmically upon h. Thus we see that in the slender-body limit the axisymmetric modes vary mainly with z, rather than radially, and correspond to large-negative permittivity eigenvalues.

Using (3.8), the displacement condition (3.4) gives

$$\frac{\partial\psi_0}{\partial\rho}=-\alpha\left(\frac{\partial\bar{\psi}_2}{\partial\rho}-\frac{df}{dz}\frac{dv}{dz}\right)\quad\text{at}\quad\rho=f(z). \tag{3.9}$$

Because of the singular scaling of $\mathcal{E}$, this leading balance involves the algebraic correction $\bar{\psi}_2$. From (3.2*a*) we find that the latter satisfies

$$\frac{1}{\rho}\frac{\partial}{\partial\rho}\left(\rho\frac{\partial\bar{\psi}_2}{\partial\rho}\right)+\frac{d^2v}{dz^2}=0\quad\text{for}\quad\rho<f(z). \tag{3.10}$$

Multiplication by ρ, followed by integration from $\rho=0$ to $\rho=f(z)$ and enforcing boundedness gives the derivative appearing in (3.9) as

$$\frac{\partial\bar{\psi}_2}{\partial\rho}=-\frac{f}{2}\frac{d^2v}{dz^2}\quad\text{at}\quad\rho=f(z). \tag{3.11}$$

Consider now the leading-order balance of (3.2*b*):

$$\frac{1}{\rho}\frac{\partial}{\partial\rho}\left(\rho\frac{\partial\psi_0}{\partial\rho}\right)=0. \tag{3.12}$$

Integration of (3.12) and using the leading-order continuity condition

$$\psi_0=v\quad\text{at}\quad\rho=f(z), \tag{3.13}$$

which follows from (3.3) and (3.7), yields

$$\psi_0(\rho,z;h)=v(z;h)+A(z;h)\ln\frac{\rho}{f(z)}, \tag{3.14}$$

where $A(z;h)$ is an integration function. Substituting (3.11) and (3.14) into (3.9), we find a relation between $A(z;h)$ and the other two unknowns $v(z;h)$ and $\alpha(h)$:

$$A(z;h)=\frac{\alpha(h)}{2}\frac{d}{dz}\left(f^2(z)\frac{d}{dz}v(z;h)\right). \tag{3.15}$$

(b) Outer limit and asymptotic matching

The inner potential (3.14) grows logarithmically and therefore does not directly satisfy the far-field attenuation condition (2.12). This growth is resolved by asymptotic matching with the *outer limit*: $h\to0$ with r fixed. In the outer limit the particle degenerates to the finite line segment $-1<z<1$ along the symmetry axis.

In particular, the logarithmic growth of the inner potential suggests the outer expansion

$$\psi(r,z;h) \sim \Psi_0(r,z;h) + \cdots \quad \text{as} \quad h \to 0, \tag{3.16}$$

where

$$\Psi_0(r,z;h) = \frac{1}{4\pi}\int_{-1}^{1} \frac{q(\zeta;h)}{\sqrt{r^2+(\zeta-z)^2}}\,d\zeta \tag{3.17}$$

is the potential due to monopole sources distributed along the degenerate line segment with charge density per unit length $q(z;h)$. For the purpose of matching with the inner region, we note that for $-1<z<1$ we have (see, e.g., [45, 62, 63])

$$\Psi_0(r,z;h) \sim \frac{q(z;h)}{2\pi}\ln\frac{2\sqrt{1-z^2}}{r} + \frac{1}{4\pi}\int_{-1}^{1}\frac{q(\zeta;h)-q(z;h)}{|\zeta-z|}d\zeta + O(r^2\ln r) \quad \text{as} \quad r\to 0. \tag{3.18}$$

Using (3.18), it is straightforward to match the inner potential (3.14) with the outer potential (3.17) (1-1 Van Dyke matching [40]). We thereby obtain the relations

$$A(z;h) = -\frac{q(z;h)}{2\pi}, \tag{3.19a}$$

$$v(z;h) - A(z;h)\ln f(z) = \frac{q(z;h)}{2\pi}\ln\frac{2\sqrt{1-z^2}}{h} + \frac{1}{4\pi}\int_{-1}^{1}\frac{q(\zeta;h)-q(z;h)}{|\zeta-z|}d\zeta. \tag{3.19b}$$

(c) Effective eigenvalue problem

Substituting (3.15) into (3.19*a*) and (3.19*b*) yields a coupled system of equations for the voltage $v(z;h)$ and charge line-density $q(z;h)$:

$$q(z;h) + \pi\alpha(h)\frac{d}{dz}\left(f^2(z)\frac{d}{dz}v(z;h)\right) = 0, \tag{3.20a}$$

$$v(z;h) = \frac{q(z;h)}{2\pi}\ln\frac{2\sqrt{1-z^2}}{hf(z)} + \frac{1}{4\pi}\int_{-1}^{1}\frac{q(\zeta;h)-q(z;h)}{|\zeta-z|}d\zeta. \tag{3.20b}$$

The differential equation (3.20*a*), which is essentially Gauss's law, relates the longitudinal variation of the cross-sectional electric-field flux to the charge. The integral equation (3.20*b*) is a nonlocal capacitance relation between the local voltage and the charge distribution along the particle axis. Together with appropriate boundary conditions at $z=\pm1$, (3.20) constitute an effective eigenvalue problem for the reduced eigenvalues $\alpha(h)$ and one-dimensional eigenfunctions $v(z;h)$ (or $q(z;h)$).

To determine the appropriate boundary conditions at $z=\pm1$ it is necessary to consider additional asymptotic regions close to the tips. In the appendix we identify the scalings of these *tip regions* and construct asymptotic approximations for the potential there that match with both the inner and outer regions. Besides extending the asymptotic description of the eigenfunctions to the tips, the analysis in the appendix shows that the eigenfunctions v (and hence q) are regular at $z=\pm1$. These regularity conditions, which are consistent with the degeneracy of the differential operator in (3.20*a*) as $z\to\pm1$ [cf. (2.7)], appear to close the effective eigenvalue problem.

We note that integration of (3.20*a*) in conjunction with the regularity of v at the tips yields

$$\int_{-1}^{1} q(z;h)\,dz = 0, \tag{3.21}$$

which shows that, as expected, the net polarization charge of the particle vanishes. Thus the charge accumulation in the tip regions is negligible.

(d) Logarithmic approximation

We derived the effective eigenvalue problem by collecting together logarithmically separated asymptotic terms so as to ensure an algebraic relative error. As a consequence, the effective problem remains dependent upon h through the logarithmic factor in (3.20*b*). While our focus will

be on solving the effective problem exactly, it is illuminating to first briefly consider a perturbative expansion in inverse logarithmic powers.

Indeed, inspection of (3.20) readily suggests the expansions

$$\alpha(h) \sim \acute{\alpha} \frac{1}{\ln \frac{1}{h}} + O\left(\frac{1}{\ln^2 \frac{1}{h}}\right) \tag{3.22}$$

and

$$v(z;h) \sim \tilde{v}(z) + O\left(\frac{1}{\ln \frac{1}{h}}\right), \quad q(z;h) \sim \frac{2\pi}{\ln \frac{1}{h}} \tilde{v}(z) + O\left(\frac{1}{\ln^2 \frac{1}{h}}\right), \tag{3.23}$$

where the leading-order eigenfunction $\tilde{v}(z)$ satisfies

$$\frac{d}{dz}\left(f^2(z)\frac{d}{dz}\acute{v}(z)\right) + \frac{2}{\acute{\alpha}}\acute{v}(z) = 0 \tag{3.24}$$

in conjunction with regularity at $z = \pm 1$. In light of the assumed behaviour of $f(z)$ at the tips [cf. (2.7)], the above problem for $\tilde{\alpha}$ and $\tilde{v}(z)$ constitutes a singular Sturm–Liouville problem [64]. We note that the "full" effective eigenvalue problem (3.20) is an example of a nonlocal-singular Sturm–Liouville problem.

In the particular case where the particle is a prolate spheroid, $f(z) = \sqrt{1-z^2}$ and hence (3.24) coincides with Legendre's differential equation. The eigenfunctions are then clearly the Legendre polynomials [65] with eigenvalues

$$\tilde{\alpha}^{(n)} = \frac{2}{n(n+1)}, \quad n = 1, 2, \ldots \tag{3.25}$$

In the next section we shall show that for a prolate spheroid the effective eigenvalue problem (3.20) can actually be solved exactly, in closed form, without the need to expand in inverse logarithmic powers. Building on the latter solution, we shall also develop a scheme for solving (3.20) for arbitrarily shaped particles.

4. Exact solutions to the effective eigenvalue problem

(a) Prolate spheroid

In this section we aim to solve the effective eigenvalue problem exactly, that is, without expanding the eigenvalues and eigenfunctions in inverse logarithmic powers. We first consider the case of a prolate spheroid. Thus, substituting $f(z) = \sqrt{1-z^2}$ into (3.20) gives

$$q(z;h) + \pi\alpha \frac{d}{dz}\left[\left(1-z^2\right)\frac{d}{dz}v(z;h)\right] = 0, \tag{4.1a}$$

$$v(z;h) = \frac{q(z;h)}{2\pi}\ln\frac{2}{h} + \frac{1}{4\pi}\int_{-1}^{1}\frac{q(\zeta;h)-q(z;h)}{|\zeta - z|}d\zeta. \tag{4.1b}$$

The solution in this case is based on the remarkable coincidence that the Legendre polynomials $P_n(z)$ are eigenfunctions of both the differential operator appearing in (4.1*a*), and the nonlocal operator appearing in (4.1*b*). Indeed, on the one hand we have Legendre's identity [65]

$$\frac{d}{dz}\left[\left(1-z^2\right)\frac{d}{dz}P_n(z)\right] = -n(n+1)P_n(z), \quad n = 1, 2, \ldots, \tag{4.2}$$

while, on the other hand, we have

$$\int_{-1}^{1}\frac{P_n(\zeta)-P_n(z)}{|\zeta - z|}d\zeta = -2P_n(z)\sum_{k=1}^{n}\frac{1}{k}, \quad n = 1, 2, \ldots, \tag{4.3}$$

an identity which appears frequently in the literature on slender-body theory [62, 63, 66]. Using the above two identities, we readily find the eigenvalues as

$$\alpha^{(n)}(h) = \frac{1}{n(n+1)} \frac{2}{\ln(2/h) - \sum_{k=1}^{n}(1/k)} \tag{4.4}$$

and their corresponding eigenfunctions (up to a multiplicative constant) as

$$q^{(n)}(z;h) = P_n(z), \quad v^{(n)}(z;h) = \frac{P_n(z)}{n(n+1)\pi\alpha^{(n)}(h)}, \quad n = 1, 2, \ldots. \tag{4.5}$$

Fig. 2 compares the predictions of slender-body theory and the exact eigenvalues obtained using separation of variables in spheroidal coordinates (see, for example, [34]). For fixed mode, the approximations are clearly asymptotic to the exact values in the limit $h \to 0$. For fixed h, however, the approximation deteriorates with increasing mode number; this will be discussed in §7. Fig. 2 also shows the eigenvalues for several non-axisymmetric modes (see section §5).

(b) Arbitrary body of revolution

Consider now an arbitrary thickness profile $f(z)$ that is smooth and satisfies the end conditions (2.7). For $f(z) \neq f_s(z)$, where $f_s(z) = (1 - z^2)^{1/2}$ is the thickness profile of a prolate spheroid, the differential operator in (3.20*a*) is no longer diagonalized by the Legendre Polynomials. Nevertheless, the regularity boundary conditions and (4.3) suggest expanding the eigenfunctions in Legendre Polynomials:

$$q(z;h) = \sum_{l=0}^{\infty} q_l(h) P_l(z), \quad v(z;h) = \sum_{l=0}^{\infty} v_l(h) P_l(z), \tag{4.6}$$

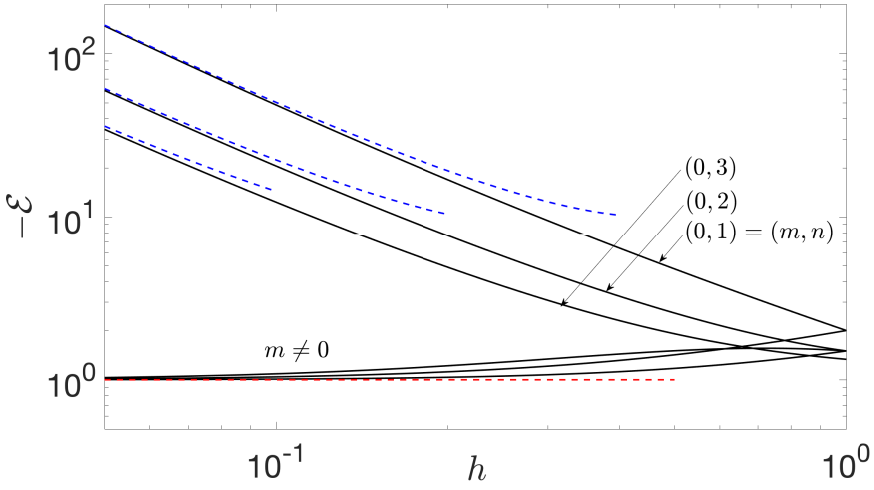

Figure 2. First few permittivity eigenvalues of a prolate spheroid: asymptotic (dashed lines) vs. exact values (solid lines). For $m = 0$ the asymptotic predictions are provided by (3.8) and (4.4); for $m \neq 0$ the eigenvalues approach the accumulation permittivity value -1 as $h \to 0$ (see §5).

where $q_0 = 0$ because of (3.21). Substituting (4.6) into (3.20), and using (2.7), orthogonality of the Legendre polynomials and integration by parts yields the algebraic system of equations

$$q_l - l(l+1)\pi\alpha v_l = \frac{1}{2}\pi\alpha(2l+1)\sum_{k=1}^{\infty} v_k \int_{-1}^{1} \frac{dP_k}{dz}\frac{dP_l}{dz}(f^2 - f_s^2)dz, \quad l = 1, 2, 3, \ldots \tag{4.7a}$$

$$v_l = \frac{1}{2\pi}\left(\ln\frac{2}{h} - \sum_{k=1}^{l}\frac{1}{k}\right) q_l + \frac{2l+1}{4\pi}\sum_{k=1}^{\infty} q_k \int_{-1}^{1} P_k P_l \ln\frac{f_s}{f} dz, \quad l = 0, 1, 2, \ldots \tag{4.7b}$$

In practice, expansions (4.6) are truncated whereby the system of equations (4.7) becomes a generalized matrix-eigenvalue problem. The latter problem is easily solved numerically for a prescribed shape function. Note that the solution procedure does not involve the zeroth equation in (4.7*b*), which is used *a posteriori* to determine v_0.

Clearly, for $f(z) = f_s(z)$ we recover the analytically solvable case of a prolate spheroid. To illustrate the solution of (4.7) we show in Fig. 3 the first three voltage eigenfunctions of a spheroid against those of a non-spheroidal shape lacking fore-aft symmetry.

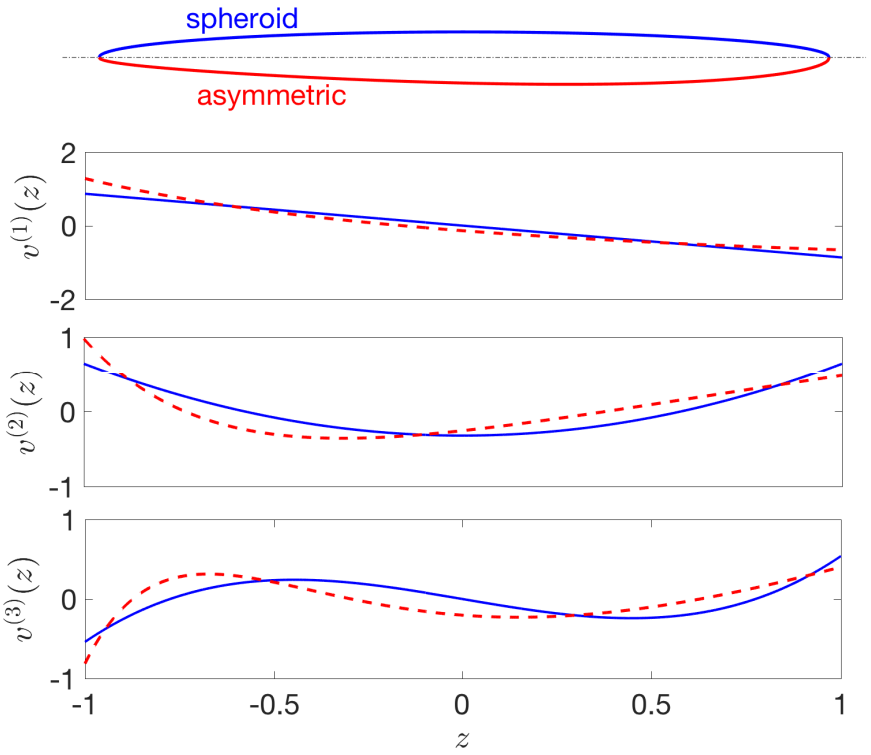

Figure 3. First three asymptotic eigenfunctions of a prolate spheroid $f(z) = (1-z^2)^{1/2}$ (solid lines) and an asymmetric shape $f(z) = (1-z^2)^{1/2}(1+z/3)$ (dashed lines) for $h = 0.07$; the corresponding approximations for the permittivity eigenvalues are respectively $-\mathcal{E} = \{86.75, 36.72, 22.39\}$ and $\{93.91, 39.97, 24.24\}$.

5. Non-axisymmetric modes

Consider next the non-axisymmetric modes ($m \neq 0$). The formulation of the inner problem is similar to that in §§2(a), only that (3.2) are generalized to [cf. (2.9*b*) and (3.1)]

$$\frac{1}{\rho}\frac{\partial}{\partial\rho}\left(\rho\frac{\partial\bar{\psi}}{\partial\rho}\right) - \frac{m^2}{\rho^2}\bar{\psi} + h^2\frac{\partial^2\bar{\psi}}{\partial z^2} = 0 \quad \text{for} \quad \rho < f(z), \tag{5.1a}$$

$$\frac{1}{\rho}\frac{\partial}{\partial\rho}\left(\rho\frac{\partial\psi}{\partial\rho}\right) - \frac{m^2}{\rho^2}\psi + h^2\frac{\partial^2\psi}{\partial z^2} = 0 \quad \text{for} \quad \rho > f(z). \tag{5.1b}$$

The reduced potentials $\bar{\psi}$ and ψ are expanded as in (3.5). At leading order, (5.1*a*) gives

$$\frac{1}{\rho}\frac{\partial}{\partial\rho}\left(\rho\frac{\partial\bar{\psi}_0}{\partial\rho}\right) - \frac{m^2}{\rho^2}\bar{\psi}_0 = 0 \quad \text{for} \quad \rho < f(z). \tag{5.2}$$

Solving (5.2) in conjunction with boundedness at $\rho = 0$ yields

$$\bar{\psi}_0(\rho, z; h) = C(z; h)\rho^m, \tag{5.3}$$

where $C(z; h)$ remains to be determined. Given the dependence of $\bar{\psi}_0$ upon ρ [cf. (3.7)], the displacement continuity condition (3.4) suggests an $O(1)$, rather than an asymptotically large, permittivity eigenvalue. Accordingly, for $m \neq 0$ we pose the eigenvalue expansion

$$\mathcal{E}(h) \sim \mathcal{E}_0(h) + \cdots \quad \text{as} \quad h \to 0. \tag{5.4}$$

The problem governing the external potential ψ_0 is obtained from the leading-order balances of (5.1*b*), (3.3) and (3.4):

$$\frac{1}{\rho}\frac{\partial}{\partial\rho}\left(\rho\frac{\partial\psi_0}{\partial\rho}\right) - \frac{m^2}{\rho^2}\psi_0 = 0 \quad \text{for} \quad \rho > f(z), \tag{5.5a}$$

$$\bar{\psi}_0 = \psi_0 \quad \text{at} \quad \rho = f(z), \tag{5.5b}$$

$$\mathcal{E}_0\frac{\partial\bar{\psi}_0}{\partial\rho} = \frac{\partial\psi}{\partial\rho} \quad \text{at} \quad \rho = f(z), \tag{5.5c}$$

together with matching with the outer region as $\rho \to \infty$. Solutions of (5.5*a*) either grow or decay algebraically with ρ; since the asymptotic order of the outer potential cannot be larger than that of the inner potential, matching implies the condition

$$\psi_0 \to 0 \quad \text{as} \quad \rho \to \infty. \tag{5.6}$$

Solving (5.5*a*) together with the continuity condtion (5.5*b*) [cf. (5.3)] yields

$$\psi_0(\rho, z; h) = C(z; h)\rho^{-m}. \tag{5.7}$$

Substitution of (5.3) and (5.7) into the displacement condition (5.5*c*) then gives

$$\mathcal{E}_0 = -1. \tag{5.8}$$

Thus, the eigenvalues corresponding to non-axisymmetric modes tend to the accumulation point of the plasmonic spectrum as $h \to 0$. This is consistent with the fact that, for fixed z, the leading-order eigenfunctions (5.3) and (5.7) are identical to the planar eigenfunctions of an infinite circular cylinder, all of which correspond to the eigenvalue -1.

It is noticeable that we did not need to determine $C(z; h)$ in order to obtain $\mathcal{E}_0$. To find $C(z; h)$, we would need to proceed to one higher order in the inner analysis and match the inner and outer regions. It is clear from (5.7) that the leading-order outer potential would involve a line distribution of dipoles, for $m = 1$, quadrupoles for $m = 2$, etc. Such an analysis would complete the description of the non-axisymmetric modes and yield the first correction in the eigenvalue expansion (5.4).

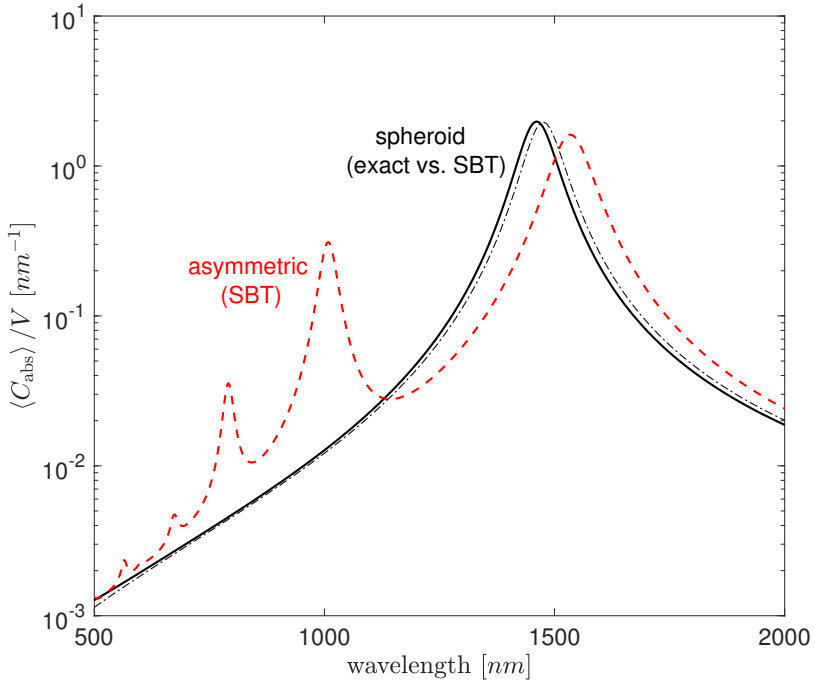

Figure 4. (a) Angle-averaged absorption cross section divided by particle volume for slender gold particles in vacuum. Exact solution for a prolate spheroid [33] (solid line); slender-body asymptotics (§6) for a prolate spheroid (dash-dotted line) and the asymmetric shape from Fig. 3 (dashed line). Parameters: $h = 0.07$, $\epsilon_b = 1$ and for $\epsilon_c(\omega)$ we use the Drude model (2.5) with $\omega_p = 1.96 \cdot 10^{16}$ (rad/sec) and $\gamma = 9.05 \cdot 10^{13}$ (rad/sec).

6. Illustration: plane-wave illumination

In this section we aim to illustrate the use of the asymptotic eigenvalues and eigenfunctions developed in §3 and §4 to study localized-surface-plasmon resonance. We focus on the scenario where an electromagnetic plane wave is incident on an axisymmetric metallic nanoparticle surrounded by vacuum; then the total potential $\varphi(\mathbf{x})$ is obtained from the spectral solution (2.4) in terms of the eigenvalues and eigenfunctions of the geometry, with $\varphi^{(i)}(\mathbf{x}) = -\mathbf{E}_\infty \cdot \mathbf{x}$ and $\epsilon_b = 1$.

Of particular interest are the optical cross-sections. In the quasi-static limit, those can be extracted from the far-field expansion of $\varphi(\mathbf{x})$,

$$\varphi(\mathbf{x}) \sim \mathbf{E}_\infty \cdot \left(-\mathbf{x} + \mathsf{M} \cdot \frac{\mathbf{x}}{4\pi|\mathbf{x}|^3} + \cdots \right) \quad \text{as} \quad |\mathbf{x}| \to \infty, \tag{6.1}$$

where M is a polarization tensor. For instance, assuming randomly oriented particles, the angle-averaged absorption cross section is given by [33]

$$\langle C_{\rm abs}\rangle = \frac{2\pi}{3\lambda} \mathrm{Im}\left(\mathrm{Tr}(\mathsf{M})\right), \tag{6.2}$$

where $\lambda = 2\pi c/\omega$, c being the speed of light in vacuum, is the wavelength of the incoming plane wave and $\mathrm{Tr}(\mathsf{M})$ denotes the trace of M.

Consider first the contributions of the axisymmetric modes to M. To this end, we inspect the far-field behaviour of the asymptotic eigenpotentials found in §3; starting from the outer solution

(3.17), and using (3.21), we find

$$\varphi^{(n,0)} \sim \frac{z}{4\pi(r^2+z^2)^{3/2}} \int_{-1}^{1} \xi q^{(n)}(\xi;h)\, d\xi \quad \text{as} \quad r^2+z^2 \to \infty. \tag{6.3}$$

Using this relation, we can evaluate the spectral solution (2.4) in the far field and compare the result with (6.1) in order to extract an asymptotic approximation for the polarization tensor; in doing so, the overlap and normalisation integrals in (2.4) are asymptotically evaluated using (3.5*b*), (3.7), (3.20*a*) and integration by parts. We thereby find

$$\mathsf{M} \sim \hat{\mathbf{e}}_z \hat{\mathbf{e}}_z \sum_n M^{(n)} \quad \text{as} \quad h \to 0, \tag{6.4}$$

where

$$M^{(n)}/a^3 = \frac{\epsilon_c(\omega)-1}{\epsilon_c(\omega)-\mathcal{E}^{(n,0)}} \frac{\left(\int_{-1}^{1} z q^{(n)}\, dz\right)^2}{\pi \alpha^{(n)} \int_{-1}^{1} \left(\frac{dv^{(n)}}{dz} f\right)^2 dz} \tag{6.5}$$

represents the contribution of the nth longitudinal mode to the polarization tensor.

In (6.5), we have [cf. (3.8)]

$$\mathcal{E}^{(n,0)} \sim -\alpha^{(n)}(h)/h^2 + \cdots, \tag{6.6}$$

where the reduced eigenvalue $\alpha^{(n)}$ is calculated as discussed in §4. From (6.6), it is clear that the longitudinal resonances of a slender particle occur when the real part of the metal permittivity scales as $-\epsilon_c' = O(1/h^2)$. In this low-frequency regime [cf. (2.5)], the imaginary part of the metal permittivity is usually large; nevertheless, as long as $\epsilon_c'' \ll 1/h^2$, (6.5) still predicts weakly damped resonances. We note that in the (unrealistic) case that ϵ_c'' is small compared to the first algebraic correction in (6.6) then the latter correction becomes important in (6.5) and needs to be considered.

In deriving (6.4) we ignored the contributions of the non-axisymmetric (transverse) modes. These contributions can be roughly estimated based on the asymptotic structure obtained in §5 together with (2.4). In particular, out interest is in the low-frequency regime $\epsilon_c = O(1/h^2)$ relevant to the excitation of the low-order axisymmetric (longitudinal) modes. In that regime, each transverse mode generally contributes to M/a^3 at $O(h)$; this is asymptotically negligible compared to the longitudinal contributions (6.5), which are typically $O(1/h^2)$ and $O(1)$ near and away from resonance, respectively. While there are infinitely many transverse modes, the contributions decay rapidly with mode number in the case of plane-wave illumination.

The integrals in the numerator of (6.5) are clearly proportional to the dipole moments of the longitudinal modes along the z direction. Referring to (4.6), the expansion of the eigenfunctions in Legendre Polynomials, it is readily seen that

$$\int_{-1}^{1} z q^{(n)}\, dz = \frac{2}{3} q_1^{(n)}. \tag{6.7}$$

Thus modes with $q_1^{(n)} = 0$ are not excited by the incident plane wave. In particular, for a spheroid $q^{(n)}(z) \propto P_n(z)$ and therefore $q_1^{(n)}$ and $M^{(n)}$ both vanish for $n \neq 1$. Thus for a spheroid only the fundamental longitudinal mode is excited; this in fact remains true also for non-slender spheroids [33]. In contrast, for non-spheroidal slender shapes $q_1^{(n)}$ does not generally vanish and we accordingly expect multiple resonances.

As an example, in Fig. 4 we compare the above predictions for a slender spheroid and the asymmetric shape studied in §§4(b). The figure also shows excellent agreement between our approximation and an exact formula for $\langle C_{\text{abs}} \rangle$ available for spheroidal particles [33].

7. Concluding remarks

We have demonstrated the use of slender-body theory (SBT) to describe the localized-surface-plasmon resonances of high-aspect-ratio nanometallic particles. For the sake of simplicity, we have assumed the quasi-static model of plasmonic resonance and a certain general class of

axisymmetric geometries. The above-mentioned assumptions, however, are in no way essential to SBT. Accordingly, we conclude with a discussion of several possible extensions to our theory. We anticipate that these extensions will provide significant insight into the plasmonic properties of complex configurations of metallic nanoparticles.

In particular, it would be relatively straightforward to generalise our scheme to particles having a curved centreline, which can be either open ended or closed, as well as to clusters of interacting particles. In fact, such geometries are routinely studied using SBT in the context of Stokes flow [37–39]. For such geometries, the outer solution is generated by distributing potential singularities along the curved centreline, which introduces more complicated nonlocal integral operators into the formulation [67]. Furthermore, we anticipate that the assumption of axial symmetry could be relaxed by use of conformal transformations to treat the quasi-two-dimensional inner problem [45].

A more subtle limitation of the class of axisymmetric geometries studied herein has to do with the manner in which the thickness profile of the particle has been prescribed, namely $r = hf(z)$ with the behaviour (2.7) at the tips. This form implies that the shape is uniformly slender, varying over a single longitudinal length scale (that of the particle); it also implies that the tips are locally paraboloidal. Under these conditions, we found an eigenvalue problem involving a singular Sturm–Liouville (SL) differential operator, supplemented by regularity conditions obtained from an analysis close to the tips.

Other classes of slender geometries include those with either pointy or blunt tips. Let us briefly consider the latter class, which is relevant to the metallic nanorod particles commonly employed in applications. Thus, consider bodies of revolution whose thickness varies on the long scale of the particle, as herein, except that close to the tips, say on the short $O(h)$ scale, the thickness rapidly vanishes. As a consequence, the differential operator in the effective eigenvalue problem is no longer singular and we anticipate that a tip analysis would provide Neumann, rather than regularity, conditions on the voltage eigenfunctions. Accordingly, to leading logarithmic order we expect a regular, rather than a singular, SL problem; for example, for a blunt-ended straight cylinder,

$$\frac{d^2\acute{v}}{dz^2} + \frac{2}{\acute{\alpha}}\acute{v} = 0, \quad \left.\frac{d\acute{v}}{dz}\right|_{z=\pm 1} = 0, \tag{7.1}$$

where we adopted the notation of (3.22)–(3.24); the eigenvalues are clearly $\acute{\alpha}^{(n)} = 8/(n\pi)^2$ $(n = 1, 2, \ldots)$ and correspond to eigenfunctions $\acute{v}^{(n)}$ harmonic in z. It would be desirable to go beyond a leading logarithmic approximation in the blunt-tip case, to calculate the eigenvalues and eigenfunctions to algebraic accuracy; the combination of Neumann conditions and the nonlocal integral operator appearing in (3.20*b*), however, would necessitate careful numerical discretization which is beyond the scope of this paper [67].

We also wish to emphasise that our analysis in §3 of the longitudinal modes is valid in the slender-body limit $h \to 0$ *for a fixed mode*. Conversely, fixing h, the longitudinal modes vary faster and faster along the particle axis, on a scale $O(a/n)$, as we increase the mode number n; accordingly, the scale disparity between the longitudinal variations and the thickness is reduced and we expect the slender-body approximation to quickly deteriorate (as indeed observed in §§4(a)). In the latter high-mode-number limit, one of us recently derived a two-term eigenvalue quantisation rule for a general class of smooth axisymmetric particles, using WKBJ methods and matched asymptotic expansions [68]. In order to connect the present theory, for n fixed, with the latter one, for h fixed, it would be necessary to consider the intermediate limit $n = O(1/h)$.

Lastly, we anticipate that our plasmonic SBT could be extended to more general physical scenarios. In particular, let us fix the aspect ratio h and consider the process of either decreasing or increasing the particle characteristic thickness ha. In the former process, as ha becomes comparable to the subnanometric Fermi-screening length, the local permittivity model used herein fails to describe the polarisation of the metal's electron gas; in that case, quantum nonlocality and electron-spillage effects may need to be considered [16, 69]. In the opposite process, the quasi-static formulation of localized-surface-plasmon resonance breaks down as

the particle length $2a$ becomes comparable to the optical wavelength. In that case, the present theory could be extended starting from a generalized spectral decomposition based on Maxwell's equations [59, 70, 71]; the outer solution would be constructed by distributing retarded singular solutions along the centreline [72], while the inner analysis would remain partially quasi-static owing to the subwavlenegth scale of the cross-section. For collections of particles, or metamaterials formed of slender particles [73, 74], retardation may be important even for deeply subwavlength particles, especially when inter-particle distances are comparable to the wavelength. In that case, each particle could be described quasi-statically, with standard multiple-scattering techniques used to study the collective response of the system [75].

Appendix: Analysis of the tip regions

(a) Rescaling and parabolic coordinates

Close to the tips, both the inner and outer expansions derived in §3 break down. Specifically, the locally parabolic behaviour (2.7) of the shape function $f(z)$ suggests considering tip regions, where both r and $|z \pm 1|$ are $O(h^2)$. In those regions, the transverse and longitudinal variations of the potential are comparably rapid (unlike in the inner region), whereas the details of the boundary shape remain discernible (unlike in the outer region).

We choose to analyse the tip region near $z = -1$. The analysis of the other tip region is similar. To this end, we consider the limit $h \to 0$ with the stretched coordinates

$$R = r/h^2, \quad Z = (z+1)/h^2 \tag{A 2}$$

fixed. Under this rescaling, the boundary is to leading order the paraboloid $Z = R^2/\kappa_-^2$ [cf. (2.7)]. This suggests the use of paraboloidal coordinates (σ, τ, θ) [76], defined through the relations

$$Z - \frac{\kappa_-^2}{4} = \frac{\tau^2 - \sigma^2}{2}, \quad R = \tau\sigma; \tag{A 3}$$

fixed (non-negative) values of either σ or τ correspond to confocal paraboloids of revolution having the symmetry axis as their axis of rotation and their foci at $(R, Z) = (0, \kappa_-^2/4)$. In terms of these coordinates, the particle boundary (2.6) can be written as $\sigma = S(\tau, h)$, wherein

$$S(\tau; h) \sim \sigma_0 + \cdots \quad \text{as} \quad h \to 0 \tag{A 4}$$

and $\sigma_0 = \kappa_-/\sqrt{2}$; the interior and exterior domains respectively become $\sigma \lesseqgtr S(\tau; h)$.

We write the internal and external tip-region potentials as $\psi = \Phi(\sigma, \tau; h)$ and $\bar{\psi} = \bar{\Phi}(\sigma, \tau; h)$, respectively; these satisfy Laplace's equation [cf. (3.2)]

$$\frac{1}{\sigma}\frac{\partial}{\partial\sigma}\left(\sigma\frac{\partial\bar{\Phi}}{\partial\sigma}\right) + \frac{1}{\tau}\frac{\partial}{\partial\tau}\left(\tau\frac{\partial\bar{\Phi}}{\partial\tau}\right) = 0 \quad \text{for} \quad \sigma < S(\tau; h), \tag{A 5a}$$

$$\frac{1}{\sigma}\frac{\partial}{\partial\sigma}\left(\sigma\frac{\partial\Phi}{\partial\sigma}\right) + \frac{1}{\tau}\frac{\partial}{\partial\tau}\left(\tau\frac{\partial\Phi}{\partial\tau}\right) = 0 \quad \text{for} \quad \sigma > S(\tau; h), \tag{A 5b}$$

the transmission conditions [cf. (3.3), (3.4) and (3.8)]

$$\bar{\Phi} = \Phi \quad \text{at} \quad \sigma = S(\tau; h), \tag{A 6a}$$

$$\left(-\frac{\alpha}{h^2} + \cdots\right)\left(\frac{\partial\bar{\Phi}}{\partial\sigma} - \frac{dS}{d\tau}\frac{\partial\bar{\Phi}}{\partial\tau}\right) = \frac{\partial\Phi}{\partial\sigma} - \frac{dS}{d\tau}\frac{\partial\Phi}{\partial\tau} \quad \text{at} \quad \sigma = S(\tau; h), \tag{A 6b}$$

as well as asymptotic matching with both the inner and outer regions (in the limits $\tau \to \infty$ and $\sigma \to \infty$, respectively).

(b) Tip interior

The large eigenvalue in the displacement condition (A 6*b*) suggests that, to leading order, the interior potential $\bar{\Phi}$ satisfies a homogeneous Neumann boundary condition on the nominal

paraboloid $\sigma = \sigma_0$. This, in turn, implies that $\bar{\Phi}$ is approximately uniform. Otherwise, (A 5*a*) in conjunction with the said Neumann condition would give solutions that exponentially grow as $Z \to \infty$; it would not be possible to match the latter behaviour to the inner region.

The above argument assumes that $\bar{\Phi}$ and Φ are comparable in magnitude, as intuitively suggested by the continuity condition (A 6*a*). It can be shown that an alternative balance of the displacement condition (A 6*b*), with $\Phi \gg \bar{\Phi}$ and the leading approximation for Φ vanishing over the nominal boundary, does not allow matching the external tip potential Φ with both the inner and outer regions; this will also become evident from the analysis in §§7(c).

With the conclusion that $\bar{\Phi}$ is approximately uniform, leading-order matching with the inner region suggests that the internal potential $\bar{\Phi}$ possesses the expansion

$$\bar{\Phi}(\sigma, \tau; h) \sim v(-1; h) + \cdots \quad \text{as} \quad h \to 0, \tag{A 7}$$

which is consistent with the proposed regularity condition on $v(z; h)$ used to solve the effective eigenvalue problem (see §§3(c)). To further corroborate this condition, and to complete the leading-order description of the tip region, we next construct an asymptotic approximation to the exterior potential Φ that is consistent with (A 7) and successfully matches with both the inner and outer expansions.

(c) Tip exterior

Consider now the domain exterior to the tip. The continuity condition (A 6*a*), together with (A 7), suggests the expansion

$$\Phi(\sigma, \tau; h) \sim \Phi_0(\sigma, \tau; h) + \cdots \quad \text{as} \quad h \to 0, \tag{A 8}$$

where Φ_0 satisfies Laplace's equation

$$\frac{1}{\sigma}\frac{\partial}{\partial \sigma}\left(\sigma \frac{\partial \Phi_0}{\partial \sigma}\right) + \frac{1}{\tau}\frac{\partial}{\partial \tau}\left(\tau \frac{\partial \Phi_0}{\partial \tau}\right) = 0, \tag{A 9}$$

the Dirichlet condition

$$\Phi_0(\sigma_0, \tau; h) = v(-1; h) \tag{A 10}$$

and conditions implied by asymptotic matching of the tip region with the inner and outer regions.

Subject to verification by matching, we attempt a solution in the form $\Phi_0(\sigma, \tau; h) = \Phi_0(\sigma; h)$; we then readily obtain from (A 9) and (A 10) that

$$\Phi_0(\sigma, \tau; h) = v(-1; h) + B(h) \ln \frac{\sigma}{\sigma_0}, \tag{A 11}$$

where $B(h)$ is a constant to be determined.

To that end, we apply 1-1 Van Dyke matching between the (exterior) tip region and the inner region. Thus, writing (A 11) in terms of the inner coordinates (ρ, z) and expanding up to leading algebraic order in h gives $v(-1; h) + B(h) \ln \rho / (\kappa_-(z+1)^{1/2})$ [cf. (3.1), (A 2) and (A 3) and note that $\sigma \sim R/(2Z)^{1/2}$ for large τ (or Z)]. This expression is required to agree with (3.14), written in terms of the tip coordinates (R, Z) and then expanded up to leading algebraic order in h. We thereby find

$$B(h) = -\frac{q(-1; h)}{2\pi}. \tag{A 12}$$

It remains to verify that the solution (A 11), with (A 12), also satisfies matching with the outer region. For this, we require the expansion of the leading-order outer potential (3.17) as the tip is approached; using standard methods for asymptotically evaluating integrals [45], we find

$$\Psi_0(r, z; h) \sim \frac{q(-1; h)}{4\pi} \ln \frac{4}{t(1 + \cos\vartheta)} + \frac{1}{4\pi}\int_{-1}^{1} \frac{q(\zeta; h) - q(-1; h)}{|\zeta + 1|} d\zeta \quad \text{as} \quad t \to 0, \tag{A 13}$$

where $t = \sqrt{r^2 + (z+1)^2}$ and ϑ denotes the polar angle from $(r, z) = (0, -1)$ with $\vartheta = 0$ corresponding to the negative z direction. Conversely, for the purpose of expanding the tip

solution (A 11) for large distances, we note that $\sigma \sim T^{1/2}\sqrt{1+\cos\vartheta}$ as $T = \sqrt{R^2+Z^2} \to \infty$. Using these two expansions, together with the limit of (3.20*b*) as $z \to -1$, it is readily verified that 1-1 Van Dyke matching between the tip and outer expansions is identically satisfied.

Data Accessibility. The code used in §4 and §6 is available at https://github.com/Matias-Ruiz/SBT-plasmonics

Authors' Contributions. The authors carried out the analysis and wrote the paper jointly. OS initiated and supervised the project. MR conducted all of the numerical investigations.

Funding. The authors acknowledge funding from EPSRC UK (New Investigator Award EP/R041458/1).

Acknowledgements. None.

References

1 Maier SA. 2007 *Plasmonics: fundamentals and applications*. Springer Science & Business Media.
2 Schuller JA, Barnard ES, Cai W, Jun YC, White JS, Brongersma ML. 2010 Plasmonics for extreme light concentration and manipulation. *Nat. Mater.* **9**, 193–204.
3 Fernández-Domingíez AI, Maier SA, Pendry JB. 2010 Collection and concentration of light by touching spheres: a transformation optics approach. *Phys. Rev. Lett.* **105**, 266807.
4 Aubry A, Lei DY, Fernández-Domingíez AI, Sonnefraud Y, Maier SA, Pendry JB. 2010 Plasmonic light-harvesting devices over the whole visible spectrum. *Nano lett.* **10**, 2574–2579.
5 Kraft M, Pendry JB, Maier SA, Luo Y. 2014 Transformation optics and hidden symmetries. *Phys. Rev. B* **89**, 245125.
6 Perfekt K, Putinar M. 2014 Spectral bounds for the Neumann-Poincaré operator on planar domains with corners. *J. Anal. Math.* **124**, 39–57.
7 Bonnetier E, Zhang H. 2017 Characterization of the essential spectrum of the Neumann-Poincaré operator in 2D domains with corner via Weyl sequences. *arXiv preprint arXiv:1702.08127*.
8 Bonnetier E, Dapogny C, Triki F, Zhang H. 2019 The plasmonic resonances of a bowtie antenna. *Anal. Theory Appl.*
9 Klimov VV, Guzatov DV. 2007 Strongly localized plasmon oscillations in a cluster of two metallic nanospheres and their influence on spontaneous emission of an atom. *Phys. Rev. B* **75**, 024303.
10 Aubry A, Lei DY, Maier SA, Pendry JB. 2010 Interaction between plasmonic nanoparticles revisited with transformation optics. *Phys. Rev. Lett.* **105**, 233901.
11 Aubry A, Lei DY, Maier SA, Pendry JB. 2011 Plasmonic hybridization between nanowires and a metallic surface: a transformation optics approach. *ACS nano* **5**, 3293–3308.
12 Lebedev VV, Vergeles SS, Vorobev PE. 2013 Surface modes in metal–insulator composites with strong interaction of metal particles. *Appl. Phys. B* **111**, 577–588.
13 Pendry JB, Fernández-Domingíez AI, Luo Y, Zhao R. 2013 Capturing photons with transformation optics. *Nature Phys.* **9**, 518–522.
14 Schnitzer O. 2015 Singular perturbations approach to localized surface-plasmon resonance: Nearly touching metal nanospheres. *Phys. Rev. B* **92**, 235428.
15 Schnitzer O, Giannini V, Craster RV, Maier SA. 2016a Asymptotics of surface-plasmon redshift saturation at subnanometric separations. *Phys. Rev. B* **93**, 041409.
16 Schnitzer O, Giannini V, Maier SA, Craster RV. 2016b Surface plasmon resonances of arbitrarily shaped nanometallic structures in the small-screening-length limit. *Proc. R. Soc. A* **472**, 20160258.
17 Schnitzer O. In press. Asymptotic approximations for the plasmon resonances of nearly touching spheres. *Eur. J. Appl. Math.*
18 Yu S, Ammari H. 2018 Plasmonic interaction between nanospheres. *SIAM Rev.* **60**, 356–385.
19 Yu S, Ammari H. 2019 Hybridization of singular plasmons via transformation optics. *Proc. Natl. Acad. Sci. U.S.A.* p. 201902194.
20 Ueno K, Juodkazis S, Mizeikis V, Sasaki K, Misawa H. 2006 Spectrally-resolved atomic-scale length variations of gold nanorods. *J. Am. Chem. Soc.* **128**, 14226–14227.

21 Chang WS, Ha JW, Slaughter LS, Link S. 2010 Plasmonic nanorod absorbers as orientation sensors. *Proc. Natl. Acad. Sci. U.S.A.* **107**, 2781–2786.
22 Bryant GW, Garcia de Abajo FJ, Aizpurua J. 2008 Mapping the plasmon resonances of metallic nanoantennas. *Nano Lett.* **8**, 631–636.
23 Chen H, Shao L, Li Q, Wang J. 2013 Gold nanorods and their plasmonic properties. *Chem. Soc. Rev.* **42**, 2679–2724.
24 Cao J, Sun T, Grattan. KT. 2014 Gold nanorod-based localized surface plasmon resonance biosensors: A review. *Sensors and Actuators B: Chemical* **195**, 332–351.
25 Huang X, El-Sayed IH, Qian W, El-Sayed MA. 2006 Cancer cell imaging and photothermal therapy in the near-infrared region by using gold nanorods. *J. Am. Chem. Soc.* **128**, 2115–2120.
26 Link S, El-Sayed MA. 1999 Spectral Properties and Relaxation Dynamics of Surface Plasmon Electronic Oscillations in Gold and Silver Nanodots and Nanorods. *J. Phys. Chem. B* **103**, 8410–8426.
27 Sönnichsen C, Franzl T, Wilk T, von Plessen G, Feldmann J, Wilson OV, Mulvaney P. 2002 Drastic reduction of plasmon damping in gold nanorods. *Phys. Rev. Lett.* **88**, 077402.
28 Prescott S, Mulvaney P. 2006 Gold nanorod extinction spectra. *J. Appl. Phys.* **99**, 123504.
29 Khlebtsov BN, Khlebtsov NG. 2007 Multipole plasmons in metal nanorods: scaling properties and dependence on particle size, shape, orientation, and dielectric environment. *J. Phys. Chem. C* **111**, 11516–11527.
30 Neubrech F, Pucci A, Cornelius TW, Karim S, García-Etxarri A, Aizpurua J. 2008 Resonant plasmonic and vibrational coupling in a tailored nanoantenna for infrared detection. *Phys. Rev. Lett.* **101**, 157403.
31 Lu G, Zhang T, Li W, Hou L, Liu J, Gong Q. 2011 Single-molecule spontaneous emission in the vicinity of an individual gold nanorod. *J. Phys. Chem. C* **115**, 15822–15828.
32 Agha YO, Demichel O, Girard C, Bouhelier A, des Francs GC. 2014 Near-Field Properties of Plasmonic Nanostructures with High Aspect Ratio. *Prog. Electromagn. Res.* **146**, 77–89.
33 Bohren CF, Huffman DR. 2008 *Absorption and scattering of light by small particles*. John Wiley & Sons.
34 Klimov VV. 2014 *Nanoplasmonics*. CRC Press.
35 Tillett JPK. 1970 Axial and Transverse Stokes Flow Past Slender Axisymmetric Bodies. *J. Fluid Mech.* **44**, 401–418.
36 Batchelor G. 1970 Slender-body theory for particles of arbitrary cross-section in Stokes flow. *J. Fluid Mech.* **44**, 419–440.
37 Cox RG. 1970 The motion of long slender bodies in a viscous fluid Part 1. General theory. *J. Fluid Mech.* **44**, 791?810.
38 Keller JB, Rubinow SI. 1976 Slender-body theory for slow viscous flow. *J. Fluid Mech.* **75**, 705–714.
39 Johnson RE. 1980 An improved slender-body theory for Stokes flow. *J. Fluid Mech.* **99**, 411–431.
40 Van Dyke MD. 1975 *Perturbation methods in fluid dynamics*. Parabolic Press.
41 Handelsman RA, Keller JB. 1967 Axially symmetric potential flow around a slender body. *J. Fluid Mech.* **28**, 131–147.
42 Newman JN. 1970 Applications of slender-body theory in ship hydrodynamics. *Annu. Rev. Fluid Mech.* **2**, 67–94.
43 Kevorkian J, Cole JD. 2013 *Perturbation methods in applied mathematics* vol. 34. Springer Science & Business Media.
44 Lauga E, Powers TR. 2009 The hydrodynamics of swimming microorganisms. *Rep. Prog. Phys.* **72**, 096601.
45 Hinch EJ. 1991 *Perturbation methods*. Cambridge university press.
46 Landau LD, Bell JS, Kearsley MJ, Pitaevskii LP, Lifshitz EM, Sykes JB. 1984 *Electrodynamics of continuous media* vol. 8. Elsevier.
47 Bergman DJ. 1979 Dielectric constant of a two-component granular composite: A practical scheme for calculating the pole spectrum. *Phys. Rev. B* **19**, 2359.
48 Ouyang F, Isaacson M. 1989 Surface plasmon excitation of objects with arbitrary shape and dielectric constant. *Philos. Mag.* **60**, 481–492.

49 Fredkin DR, Mayergoyz ID. 2003 Resonant behavior of dielectric objects (electrostatic resonances). *Phys. Rev. Lett.* **91**, 253902.
50 Bergman DJ, Stockman MI. 2003 Surface plasmon amplification by stimulated emission of radiation: quantum generation of coherent surface plasmons in nanosystems. *Phys. Rev. Lett.* **90**, 027402.
51 Mayergoyz ID. 2013 *Plasmon resonances in nanoparticles* vol. 6. World Scientific.
52 Mayergoyz ID, Fredkin DR, Zhang Z. 2005 Electrostatic (plasmon) resonances in nanoparticles. *Phys. Rev. B* **72**, 155412.
53 Li K, Stockman MI, Bergman DJ. 2005 Enhanced second harmonic generation in a self-similar chain of metal nanospheres. *Phys. Rev. B* **72**, 153401.
54 Grieser D. 2014 The plasmonic eigenvalue problem. *Rev. Math. Phys.* **26**, 1450005.
55 Davis TJ, Gómez DE. 2017 Colloquium: An algebraic model of localized surface plasmons and their interactions. *Rev. Mod. Phys.* **89**, 011003.
56 Ammari H, Millien P, Ruiz M, Zhang H. 2017 Mathematical analysis of plasmonic nanoparticles: the scalar case. *Arch. Ration. Mech. Anal.* **224**, 597–658.
57 Voicu RC, Sandu T. 2017 Analytical results regarding electrostatic resonances of surface phonon/plasmon polaritons: separation of variables with a twist. *Proc. R. Soc. A* **473**, 20160796.
58 Bergman DJ, Farhi A. 2018 Spectral method for the static electric potential of a charge density in a composite medium. *Phys. Rev. A* **97**, 043855.
59 Chen PY, Bergman DJ, Sivan Y. 2019 Generalizing Normal Mode Expansion of Electromagnetic Green's Tensor to Open Systems. *Phys. Rev. Appl.* **11**, 044018.
60 Johnson PB, Christy RW. 1972 Optical constants of the noble metals. *Phys. Rev. B* **6**, 4370.
61 Crighton DG, Leppington FG. 1973 Singular perturbation methods in acoustics: diffraction by a plate of finite thickness. *Proc. R. Soc. A* **335**, 313–339.
62 Tuck E. 1964 Some methods for flows past blunt slender bodies. *J. Fluid Mech.* **18**, 619–635.
63 Tuck EO. 1992 Analytic aspects of slender body theory. *Wave asymptotics* pp. 184–201.
64 Zettl A. 2005 *Sturm-Liouville Theory* vol. 121. Mathematical Surveys and Monographs, American Mathematical Society.
65 Abramowitz M, Stegun IA. 1972 *Handbook of mathematical functions*. Dover New York.
66 Blake JR, Tuck EO, Wakeley PW. 2010 A note on the S-transform and slender body theory in Stokes flow. *IMA J. Appl. Math.* **75**, 343–355.
67 Tornberg AK, Shelley MJ. 2004 Simulating the dynamics and interactions of flexible fibers in Stokes flows. *J. Comput. Phys.* **196**, 8–40.
68 Schnitzer O. 2019 Geometric quantization of localized surface plasmons. *IMA J. Appl. Math.* **84**, 813–832.
69 Luo Y, Fernández-Domingíez AI, Wiener A, Maier SA, Pendry JB. 2013 Surface plasmons and nonlocality: a simple model. *Phys. Rev. Lett.* **111**, 093901.
70 Bergman DJ, Stroud D. 1980 Theory of resonances in the electromagnetic scattering by macroscopic bodies. *Phys. Rev. B* **22**, 3527.
71 Agranovich MS, Katsenelenbaum BZ, Sivov AN, Voitovich NN. 1999 *Generalized method of eigenoscillations in diffraction theory*. Wiley-VCH Pub.
72 Geer J. 1980 Electromagnetic scattering by a slender body of revolution: axially incident plane wave. *SIAM J. App. Math.* **38**, 93–102.
73 Aizpurua J, Bryant GW, Richter LJ, De Abajo FJG, Kelley BK, Mallouk T. 2005 Optical properties of coupled metallic nanorods for field-enhanced spectroscopy. *Phys. Rev. B* **71**, 235420.
74 Kabashin AV, Evans P, Pastkovsky S, Hendren W, Wurtz GA, Atkinson R, Pollard R, Podolskiy VA, Zayats AV. 2009 Plasmonic nanorod metamaterials for biosensing. *Nat. Mater.* **8**, 867.
75 Martin PA. 2006 *Multiple scattering: interaction of time-harmonic waves with N obstacles*. Cambridge University Press.
76 Happel J, Brenner H. 2012 *Low Reynolds number hydrodynamics: with special applications to particulate media* vol. 1. Springer Science & Business Media.